



# Thermal analysis during solidification of an Al–Cu eutectic alloy: interrelation of thermal parameters, microstructure and hardness

Rafael Kakitani<sup>1</sup> · Guilherme Lisboa de Gouveia<sup>2</sup> · Amauri Garcia<sup>1</sup> · Noé Cheung<sup>1</sup> · José E. Spinelli<sup>2</sup> 

Received: 18 July 2018 / Accepted: 23 December 2018 / Published online: 18 January 2019  
© Akadémiai Kiadó, Budapest, Hungary 2019

## Abstract

Eutectic alloys are considered promising candidates for high-temperature structural applications. In spite of this, quantitative examination of the effect of the length scale of the eutectic microstructure on mechanical properties remains a challenge. In this sense, assessments of morphology, size and distribution of the phases forming the eutectic mixture, solidified under transient regime and different cooling conditions, endure necessary. In the present study, a large spectrum of cooling rates has been obtained during unsteady-state directional solidification of an Al–33 mass% Cu alloy. The main techniques utilized were: optical microscopy; scanning electron microscopy with X-ray energy-dispersive spectroscopy, X-ray fluorescence spectroscopy and Vickers hardness (HV). The resulting microstructures related to various solidification cooling rates are shown to be formed by eutectic colonies. Three microstructural zones constitute the colony, that is, a fine central regular lamellar Al–Al<sub>2</sub>Cu eutectic, an intermediate narrow wavy lamellar eutectic and a coarse boundary eutectic zone. Iron impurity appears to be able to degenerate the eutectic into a more randomly distributed microstructure. The colonies' morphology exhibits a transition from regular to platelike cells with the increase in cooling rate. Furthermore, the evolution of hardness as a function of the colony spacings is outlined. The highest hardness of 200 HV is related to an ultrafine bimodal structure formed by platelike eutectic colonies with 13 μm in spacing with very fine lamellae of 330 nm in spacing.

**Keywords** Eutectic · Solidification · Growth models · Alloys · Metals

## Introduction

Alloys of eutectic or near-eutectic compositions are largely employed in casting, soldering and welding processes because of their low melting points, good forming flexibility and high mechanical properties [1, 2]. For the improvement in such properties, it remains essential to trace relationships linking the solidification thermal parameters and the eutectic microstructure scale. Previous research efforts on the growth of eutectics have allowed establishing experimental relationships [3–9].

In this respect, a general quantitative expression was first proposed by Jackson and Hunt (*J–H model*) [10]. The calculations are based on solving the diffusion problem at the solid/liquid interface, and the growth model predicts that  $\lambda_E^2 v = \text{const}$ , that is, the product of the square of the eutectic spacing,  $\lambda_E$ , and the growth rate,  $v$ , is equal to a constant. In the case of the Al–Al<sub>2</sub>Cu eutectic, Çadrlı et al. [11] found  $\lambda_E^2 v = 156 \mu\text{m}^3 \text{s}^{-1}$ , Ourdjini et al. [12] reported  $164 \mu\text{m}^3 \text{s}^{-1}$  for stationary slow cooling conditions ( $v < 0.4 \text{ mm s}^{-1}$ ), while Zimmerman et al. [13] found a  $\lambda_E^2 v = 88 \mu\text{m}^3 \text{s}^{-1}$  during fast cooling ( $v > 10 \text{ mm s}^{-1}$ ) of a laser remelting treatment. There are many discrepancies among the data reported for Al–Al<sub>2</sub>Cu eutectic growth [14]. Stoichev et al. [14] stated that a probable explanation refers to freezing conditions that are not cared of during experimentations, e.g., presence and intensity of convective flow at the solid/liquid interface or impurity influences.

The broad application of J–H constants confirms that the lamellar eutectic spacing is one of the crucial parameters of

✉ José E. Spinelli  
spinelli@ufscar.br

<sup>1</sup> Department of Manufacturing and Materials Engineering, University of Campinas UNICAMP, Campinas, SP 13083-860, Brazil

<sup>2</sup> Department of Materials Engineering, Federal University of São Carlos, São Carlos, SP 13565-905, Brazil

eutectic alloys [15]. This is explained by the effects of growth rate on the liquid diffusion coefficient ahead the solidification front as well as on the melt convection, changing  $\lambda_E$  accordingly. It is worth noting that there is a lack of research substantiated in intermediate growth rates under transient heat flow conditions, which are those closely related to the industrial practice. In the present investigation, the thermal gradient and growth rate are interdependent and vary freely with time. This is the same as typically found in industrial casting processes.

According to Zimmerman et al. [13, 16], the increase in cooling rate may propitiate various morphologies to happen in Al–Cu eutectic alloy, such as degenerated eutectic, banded structure or even amorphous Al–Cu phase. Çadırılı et al. [11] identified the presence of dendrite-like colony arrangements for their highest tested pulling rate of  $0.48 \text{ mm s}^{-1}$ . Although no measurement was taken on that matter, it was stated that the eutectic colony influenced the lamellar spacing measurement if some part of the colony was considered. It appears that the eutectic spacing variation across the eutectic colony is often not examined. Further, the eutectic spacing is generally believed to follow the same scaling relation as that for a planar eutectic interface. No detailed quantitative research work has been developed on the relationships between the unsteady-state scale of the Al–Cu eutectic colonies and the solidification thermal parameters, such as the cooling rate and the growth rate. The growth of the eutectic colony is mainly reported to be related to the presence of a ternary impurity element, which leads to the constitutional supercooling at the solidification interface [5].

Stoichev et al. [14] researched the influence of iron impurity on the Al–Cu eutectic solidification. The lamellar eutectic spacing was shown to be affected by the concentration of impurity. The larger values for an alloy modified with 0.09 mass% Fe compared with that for a 0.05 mass% Fe-containing alloy were justified by the non-uniform distribution of the iron during solidification. A previous research work [17] revealed that Fe is preferably deposited within the  $\alpha$ – $\beta$  interlamellar surfaces. The main proposition is that such deposit may change the specific surface energy. If melt movement ahead the solidification interface is not enough to equalize local iron concentration, a needlelike phase would be possibly formed [14]. The growth of these phases consumes the impurity on the solidification front, lowering its concentration. Consequently, no effect on the microstructure is expected to occur. Quite the reverse, a vigorous movement of the melt takes away from the solidification front the excess of iron atoms. As a result, no new intermetallics would appear. On the whole, it has been reported that iron additions may cause the enlargement of the lamellar structure, which is partly changed into a coarse rodlike one.

Zimmerman et al. [18] also dealt with local variations in the lamellar spacing in three hypoeutectic Al–Cu eutectic alloys with 25, 28 and 31 mass% Cu. The oscillatory eutectic was characterized in detail. It was experimentally found that the angle  $\theta$  between a boundary line and the growth direction is about  $35^\circ$ . It was stated that the breakdown of steady-state lamellar eutectic structure is not necessarily related to the appearance of dendrites of the primary phase. According to this research, the destabilization of the lamellas is first caused by the growth of an oscillatory morphology. Such structure carries on over a wide range of compositions and growth rates.

Sahoo and Ghosh [19] investigated the transient stage microstructures resulting from the strip casting process of an Al–Cu eutectic alloy. They observed the formation of a globular  $\alpha$ -Al phase within an Al–Al<sub>2</sub>Cu eutectic structure for estimated growth rates higher than  $20 \text{ mm s}^{-1}$ . Considering such fast cooling conditions, the Al–33 mass% Cu alloy exhibited off-eutectic behavior, being the extension of this behavior increased with the increase in cooling rate.

The Al–Al<sub>2</sub>Cu eutectic has been widely investigated so far [20]. A regular lamellar morphology generally characterizes its growth. However, the brittle nature of such eutectic limits its application [21–24]. Improvement in ductility may be obtained by refining the microstructure. Microstructural refinements may be achieved by reducing the interphase spacing, which is affected by either rapid solidification or alloying additions [25, 26]. However, none of the existing studies devoted to that have extended to the level of two-phase cellular structures, that is, the eutectic colonies. None of these studies examined the microstructure aspects inside the colony and their effects on mechanical strength. It appears that the control of volume fractions of the distinct morphologies forming a colony and constituent phases could provide greater flexibility in processing eutectics with a prospect of diversifying the resulting mechanical properties.

The conditions (unsteady-state ‘ $v$ ’ between  $0.2$  and  $1.6 \text{ mm s}^{-1}$ ) achieved during the present investigation are closer to those of industrial processes dealing with liquid-to-solid transformation. Based on the Al–33 mass% Cu alloy directionally solidified specimens under transient regime, the main purpose of this research work is to quantitatively characterize the growth of eutectic colonies. Various scales of the eutectic microstructure are assessed as the variation in size of the eutectic colony, the progression of the lamellar eutectic and the scale of the coarser randomly distributed zone. All scales will be associated with the range of experimental cooling rates and growth rates along the length of the directionally solidified (DS) casting. A correlation between the Vickers hardness and the colony spacing is also anticipated.

## Experimental procedure

### Thermal analysis during solidification

An unsteady-state setup was employed in order to directionally solidify the Al–33 mass% Cu alloy casting. This setup is detailedly described in previous research works [3, 6] and also in Fig. 1. The directionally solidified body shows different cooling conditions from the bottom to the top which generates varied microstructural features depending on the relative position. Commercial-purity Al (99.79 mass%) and high-purity Cu (99.9 mass%) were melted in order to prepare the alloy.

This setup operates an in situ remelting of the alloy by heating with radial electrical resistances involving an inner coated stainless steel mold. When the melt temperature achieves 10% above the eutectic temperature, i.e., 603 °C, the furnace windings were disconnected, and at the same time, the external water flow at the bottom of the container was to begin the cooling down procedure, thus permitting the onset of solidification.

The solidification setup supports the placing of a number of fine K-type thermocouples along the length of the casting. Using as reference the cooled base of the casting, a

setting of the thermocouples' tips was performed in distinct quotas until 66 mm. The temperature device permitted very accurate data acquisition of 5 Hz on each thermocouple for both cooling curve and directional solidification thermal profiles. A checking of the thermocouples' tips after solidification allowed the examination of the exact positions of measurement.

### Microstructural measurements and hardness tests

The following samples were examined through metallography: 5 mm, 10 mm, 15 mm, 20 mm, 25 mm, 30 mm, 40 mm, 50 mm, 60 mm and 70 mm from the cooled base of the DS casting. The metallographic process includes evaluation of longitudinal and transverse samples of each position, which were mounted, polished and etched with a solution of 0.5% HF in water during 15 s. After that, examination using an optical microscope was performed.

The microstructural features of each sample were assessed by using an Olympus inverted metallurgical microscope (model 41GX). The spacing between colony units represented the length scale of the eutectic colony. In addition to that, the determination of the Al<sub>2</sub>Cu spacing

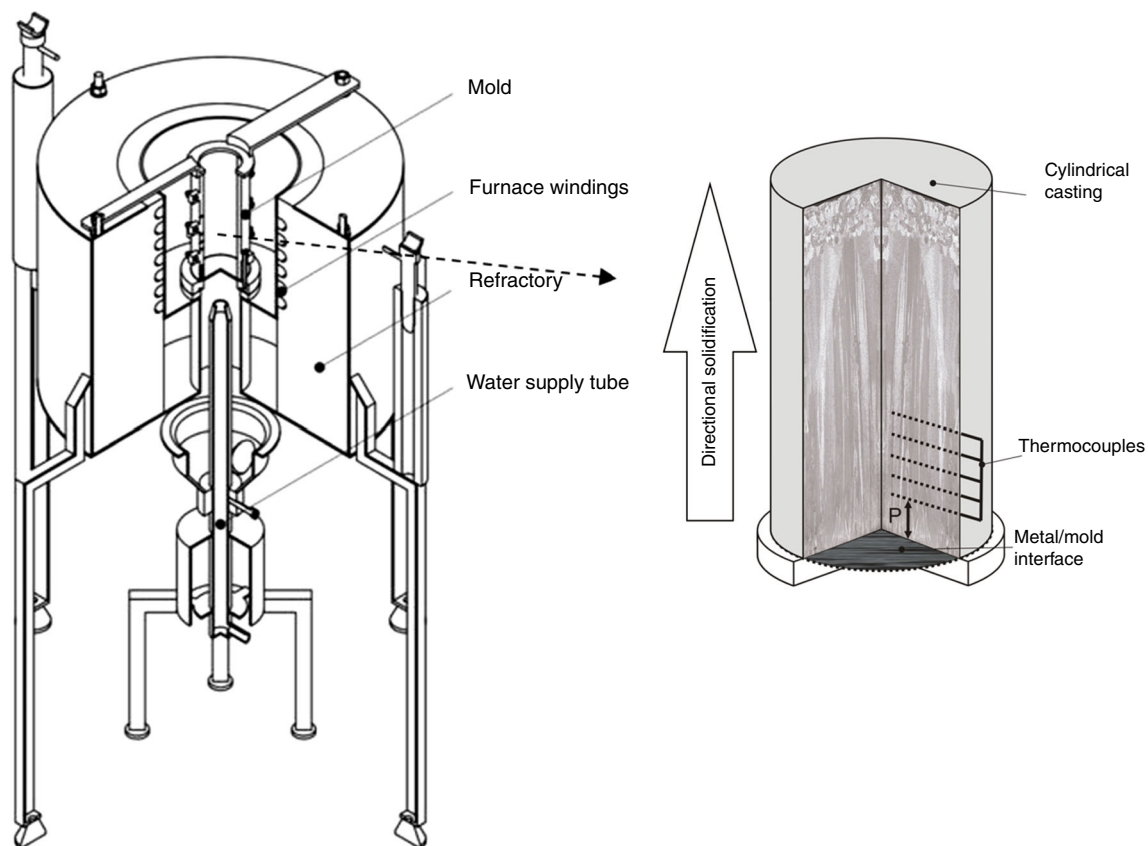


Fig. 1 Schematic representation of the casting assembly and cylindrical casting

was referred to either center lamellar eutectic or edge random eutectic shapes.

Measurements on the as-solidified microstructure were taken using the line-intercept method [27, 28] for lamellar,  $\lambda_L$ , colony spacings within the platelike region,  $\lambda_{EC}$ , and coarse random zone,  $\lambda_E$  [27]. The triangle method was employed to measure the  $\lambda_{EC}$  within the regular cells region. The schematic representation in Fig. 2 shows more clearly the methods employed to measure these spacings. For each mentioned spacing, seventy measurements were taken for each selected position in the DS casting.

Advanced characterization of the microstructures, morphologies and compositions of the phases was carried out through SEM analyses in both secondary electrons (SE) and back-scattered electron (BSE) modes. In order to enable the observation of the morphological details within the eutectic colonies, deep-etched samples were prepared (HCl during 3 min). The instrument used was a Zeiss SEM (Zeiss—EVO-MA15) equipped with an Oxford-X-Max energy-dispersive X-ray spectroscopy (EDS).

The instrument used to determine the Cu and Fe contents on the whole longitudinal section of the DS casting was a Rigaku Rix 3100 X-ray fluorescence spectrometer.

Vickers microhardness profiles were determined by using a test load of 500 g and a count time of 15 s. A Shimadzu HMV-G 20ST model hardness measuring test device was used for those measurements. The adopted Vickers hardness was the average of at least 15 measurements on each sample.

## Results and discussion

### Macrostructure, microstructures and solidification thermal variables

Figure 3a shows the equilibrium cooling curve of the Al–33 mass% Cu alloy obtained before the directional solidification test. Eutectic temperature,  $T_E$ , of 548 °C was determined in this previous experiment in which the alloy was slowly cooled in a well-insulated crucible, thus permitting the transformation temperature to be followed. In addition to that, the last 110 s during the eutectic transformation reveals a drop in the transformation temperature. The temperature decreased to 545 °C ( $T_i$ ) during such stage. According to Mondolfo [29], Fe impurity can promote two ternary phases in equilibrium with aluminum:  $(FeCu)Al_6$  and  $Cu_2FeAl_7$ . Those can be present in very low-iron Al–Cu alloys. The  $(FeCu)Al_6$  is the equivalent to the unstable  $FeAl_6$  compound. A ternary eutectic reaction is stated to take place at 545 °C for very low Fe quantity, which means ‘liquid’ into  $Al + CuAl_2 + Cu_2FeAl_7$ . It appears that the ending part of the eutectic level in Fig. 3a refers to that reaction.

The as-cast macrostructure, revealed after chemical etching of the DS Al–33Cu alloy casting, is shown in Fig. 3b. Very fine columnar grains prevailed along the entire length of the casting.

The thermocouples inserted within the Al–Cu eutectic alloy DS casting during solidification allowed to investigate the evolution of temperature versus time along the length of the casting, as shown in Fig. 4. Further, such experimental thermal profiles and the alloy eutectic

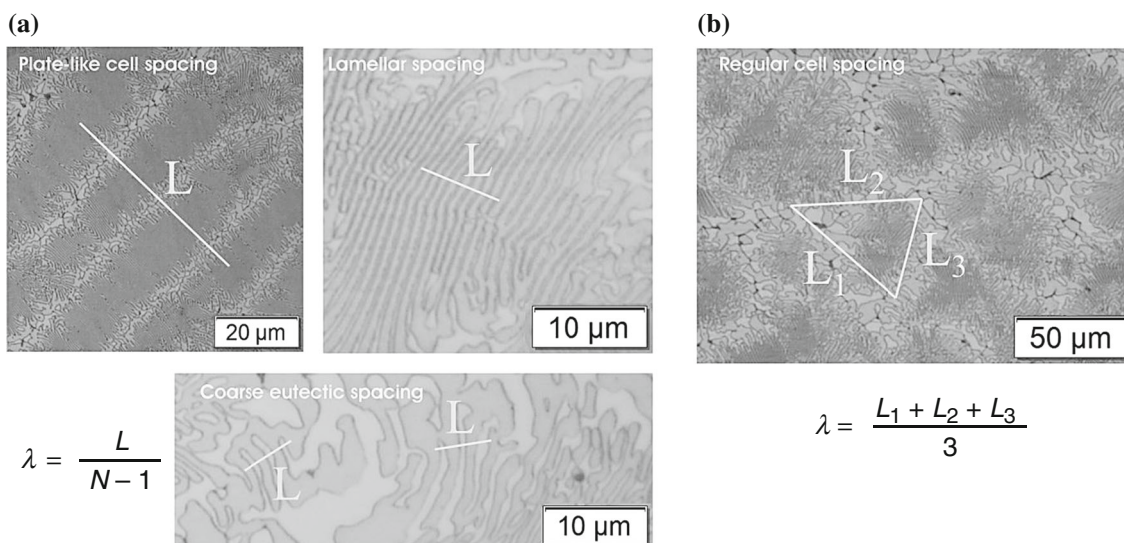


**Fig. 2** Schematic representation of transverse sections of methods used to measure microstructural spacings: **a** intercept method for  $\lambda_{EC}$ ,  $\lambda_L$  and  $\lambda_E$  and **b** triangle method for  $\lambda_{EC}$  in the regular cells regions.

‘ $L$ ’ is the length of the line and ‘ $N$ ’ is the number of intercepted phases. ‘ $L_1$ ,  $L_2$  and  $L_3$ ’ are the sides of the triangle formed considering the neighboring colonies



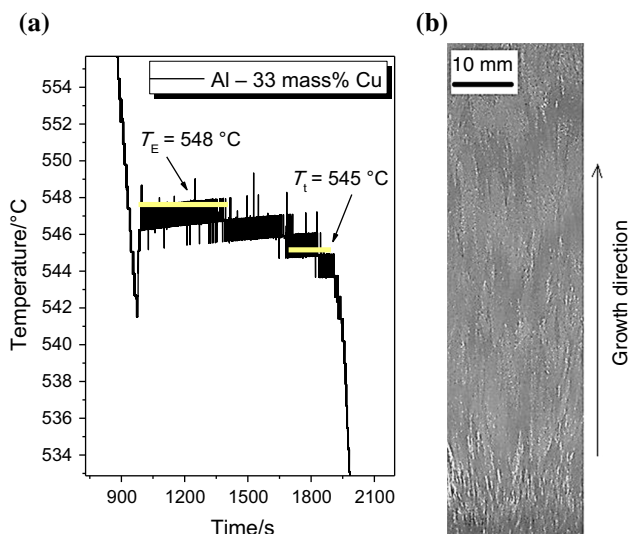


**Fig. 3** **a** Experimental time–temperature curve allowing eutectic temperatures to be determined before solidification test and **b** macrostructure of the Al–33 mass% Cu directionally solidified eutectic alloy

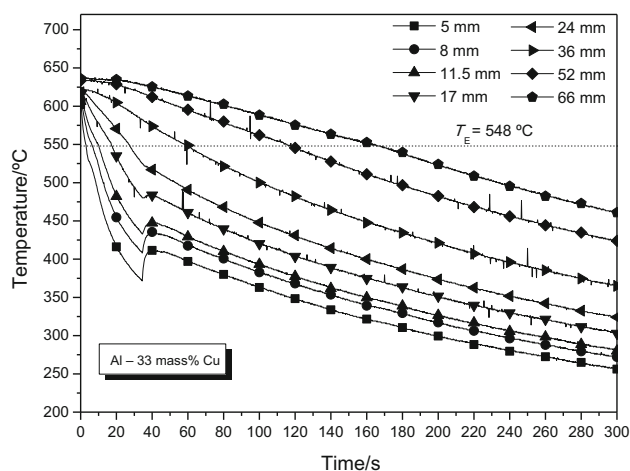


**Fig. 4** Experimental thermal profiles during transient directional solidification of the Al–33 mass% Cu eutectic alloy. Positions from the metal/mold interface are informed inside the graph

temperature ( $T_E$ ) of 548 °C, measured by thermal analysis, have been used in order to determine the solidification thermal parameters: growth rate ( $v_E$ ) and cooling rate ( $\dot{T}$ ). It is worth noting the formation of a metal/mold gap related to 40 s of processing. This is due to the intense contraction promoted by the first formed solid layer. This explains the increase in temperature observed in three thermocouples near the base of the casting. Such heating stage can be considered intrinsic to the directional solidification process, and such effect will be translated to the thermal solidification parameters.

By analyzing the longitudinal and transverse microstructures obtained by light etching procedures in

Figs. 5–7, it can be seen that eutectic cells predominate in all cases. The microstructures typified in Figs. 5–7 are associated with cooling rates of  $13.2 \text{ K s}^{-1}$ ,  $1.6 \text{ K s}^{-1}$  and  $0.7 \text{ K s}^{-1}$ , respectively. Based on the highly magnified images at the right side, a two-phase eutectic structure can be recognized. A bimodal distribution of Al–Al<sub>2</sub>Cu can be seen, that is, finer eutectic developed in the center zone of the cells and coarser eutectic at the boundaries. The growth of these so-called eutectic colonies is barely reported in the literature. Some knowledge can be learned for metallic systems such as Al–Ni [9, 30, 31], Sn–Cu [32] and Ag–Cu [33, 34].

The microstructures show a predominance of lamellar  $\alpha$ -Al + Al<sub>2</sub>Cu eutectic. But also show that there are darker gray particles decorating the boundaries of the cells, indicated by black arrows. It is quite clear that a single eutectic cell includes three microstructure zones inside itself, which are: very thin lamellas in the center, wavy lamellas and coarser random eutectic at the boundaries. The segregation of iron is the main reason for that. As observed by Stoichev et al. [14], iron may cause the enlargement of the lamellar structure. Iron is accumulated in the cells' boundaries increasing local Fe concentration, so that Fe-containing intermetallic particles could be formed. No such particles were noted in the other two zones; besides, the boundaries and the nature of these particles will be described later in this paper.

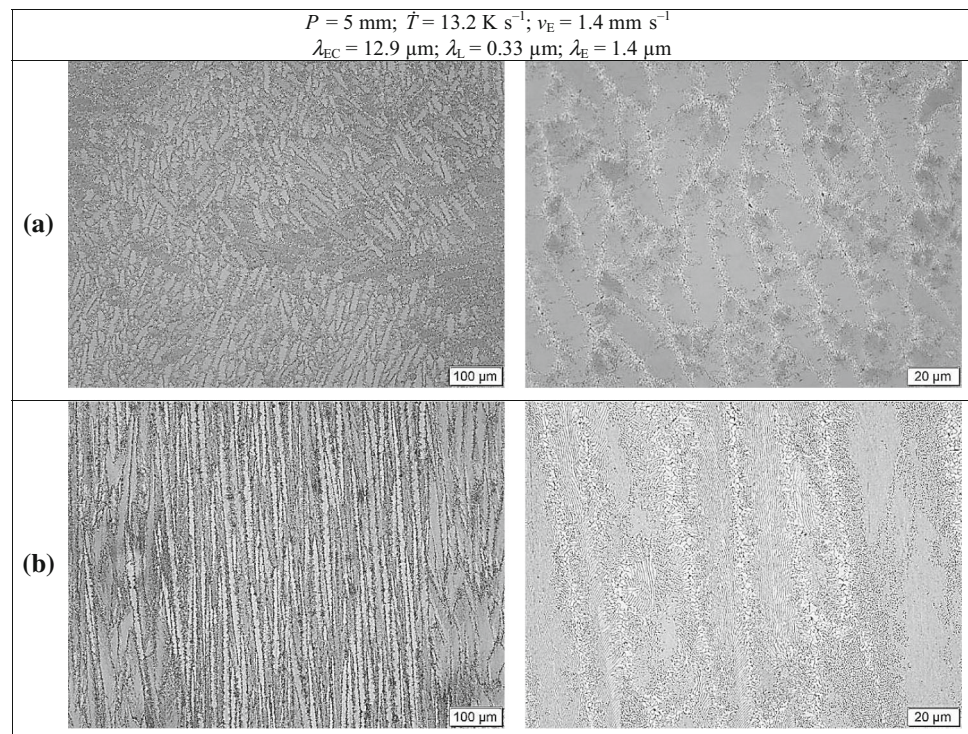
The formation of new Al<sub>2</sub>Cu coarser phase (at the cell's boundary) seems to happen with basis on a preceding wavy eutectic. This means that the morphological transition from lamellar to random shape does not occur abruptly. The fairly gradual transition is due to the wavy microstructure, which forms a narrow zone previous to the onset of the randomly distributed eutectic. Iron destabilizes the structure from the center to the edge of the cell. This is in agreement with previous works in this field. According to a few authors [35, 36], the presence of impurities can cause the breakdown of a planar eutectic interface into a cellular or colony structure.

There are indications in both the optical and the SEM microstructures (i.e., Figs. 8, 9) that the adjustment of the eutectic growth occurs through the tilting of the firstly formed phase followed by the repeated splitting of a collection of lamellas to conceive a new coarser arrangement. This process of tilting and nucleation of a new eutectic phase was shown to give rise to larger eutectic spacings, as demonstrated by Han [37].

The optical and SEM microstructures in Figs. 5–9 show coarsening of the microstructure features with the decrease in cooling rate.

Some authors [32, 38] debated that non-equilibrium during eutectic growth may be achieved if the composition immediately ahead the solidification front diverges from

**Fig. 5** Optical microstructures of the Al–33 mass% Cu alloy representing **a** transversal and **b** longitudinal features for a cooling rate of  $13.2 \text{ K s}^{-1}$  at the position  $P = 5 \text{ mm}$  from the cooled base of the casting



the equilibrium one. In this case, the solidification kinetics is more intense than the diffusion kinetics, which provokes non-conventional microstructures to be formed. In the present research with the Al–Cu eutectic alloy, solidification advanced under relatively high unsteady-state growth rates.

For monophasic alloys, it is well known that the microstructure can transition either from plane front to cells or from cells to plane front. Such transitions are related to the limit of constitutional supercooling ( $v_c$ ) and to the limit of absolute stability ( $v_a$ ) for low-velocity and high-velocity cells, respectively [39]. Xu et al. [40] stated that the growth of ‘high-velocity platelike cells’ in Zn–Ag alloys is an intermediate stage characterizing transition from regular cells to a plane front. This has been proved for either stationary solidified or laser remelted Zn–0.6% and 1.8% Ag alloys specimens. Such research affirmed that the formation of Zn-rich plates depends on the growth rate. However, the validity of such concepts regarding the micromorphology of two-phase cellular structures remains undetermined.

In the present investigation, the growth of platelike eutectic cells is shown in Fig. 5 for regions close to the cooled surface of the casting that is associated with higher eutectic cooling rates of  $13.2 \text{ K s}^{-1}$ . The platelike cellular morphology in the Al–Cu eutectic alloy prevailed for  $v_E > 0.6 \text{ mm s}^{-1}$ . Considering that the evaluation of stability of eutectic cells configurations is very scarce, a

comparison of the present results with those of monophasic microstructures seems reasonable.

For example, Ma et al. [41] observed a transition from regular cells to platelike cells for a Zn–1.52 mass% Cu alloy when the growth velocity exceeded  $1.0 \text{ mm s}^{-1}$ . Another study [42] revealed that the morphology of the Zn-rich phase for Zn–0.3 mass% Mg and Zn–0.5 mass% Mg alloys predominated as being platelike cells for  $v > 0.8 \text{ mm s}^{-1}$  and  $v > 1.5 \text{ mm s}^{-1}$ , respectively. Platelike cells were reported to be dominant for ‘ $v$ ’ higher than  $1.0 \text{ mm s}^{-1}$  and  $2.4 \text{ mm s}^{-1}$  for Zn–0.6 at% Ag and Zn–1.8 at% Ag alloys, respectively [40]. In the present results, platelike cells started to prevail for  $v > 0.6 \text{ mm s}^{-1}$ , which is lower than the aforementioned ones. The eutectic nature of the Al–Al<sub>2</sub>Cu cells seems to anticipate the regular → platelike cells transition as compared to what happens for monophasic alloys. This is quite acceptable considering that eutectics tend to grow following a plane solid/liquid interface and, in the case of the eutectic colonies formed in the Al–33 mass% Cu alloy, the growth of a platy structure for  $0.6 \text{ mm s}^{-1} < v < 1.4 \text{ mm s}^{-1}$  could precede the stability of the front for growth rates exceeding such range.

The cooling curves of Fig. 4 were used to combine pairs of values of position ( $P$ ), from the metal/mold interface, and related time ( $t_E$ ) of the eutectic front passing by each thermocouple, i.e.,  $P = f(t_E)$ . A time derivative of a generated function with those values was estimated so that the eutectic growth rate ( $v_E$ ) could be determined. In addition to that, a time derivative of each cooling curve ( $dT/dt$ ) in



**Fig. 6** Optical microstructures of the Al–33 mass% Cu alloy representing **a** transversal and **b** longitudinal features for a cooling rate of  $1.6 \text{ K s}^{-1}$  at the position  $P = 30 \text{ mm}$  from the cooled bottom of the casting

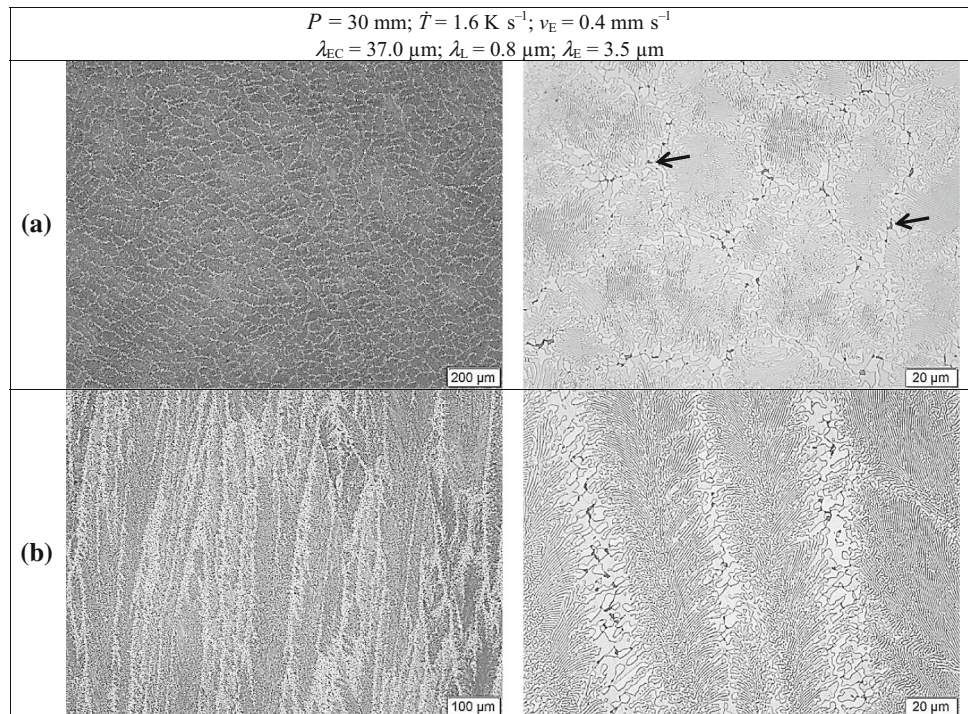


**Fig. 7** Optical microstructures of the Al–33 mass% Cu alloy representing **a** transversal and **b** longitudinal features for a cooling rate of  $0.7 \text{ K s}^{-1}$  at the position  $P = 60 \text{ mm}$  from the cooled bottom of the casting

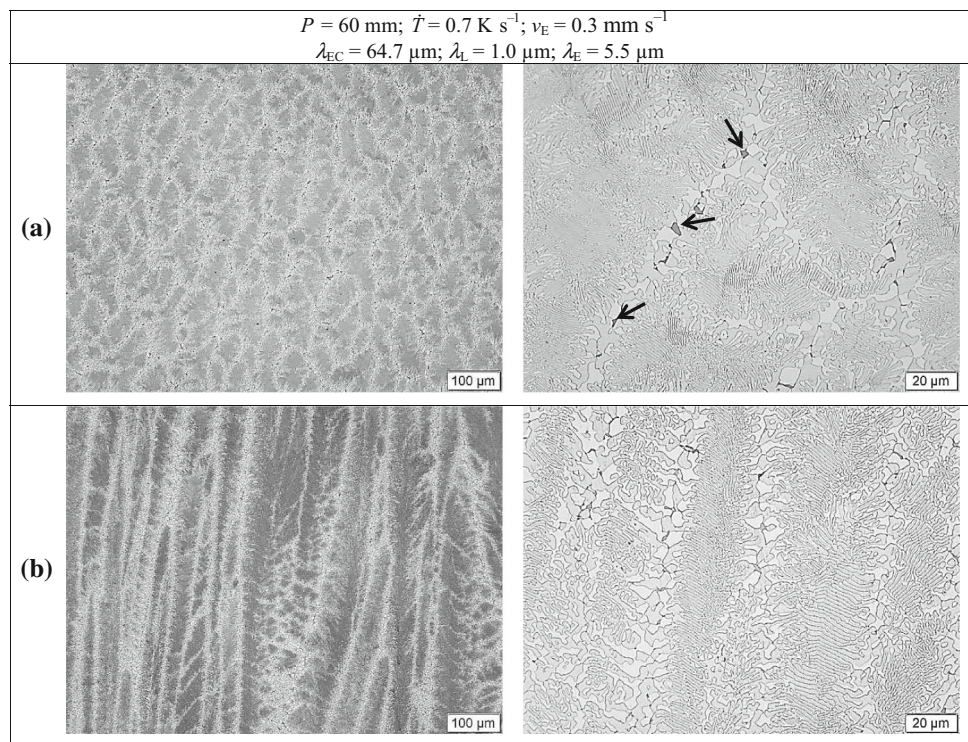
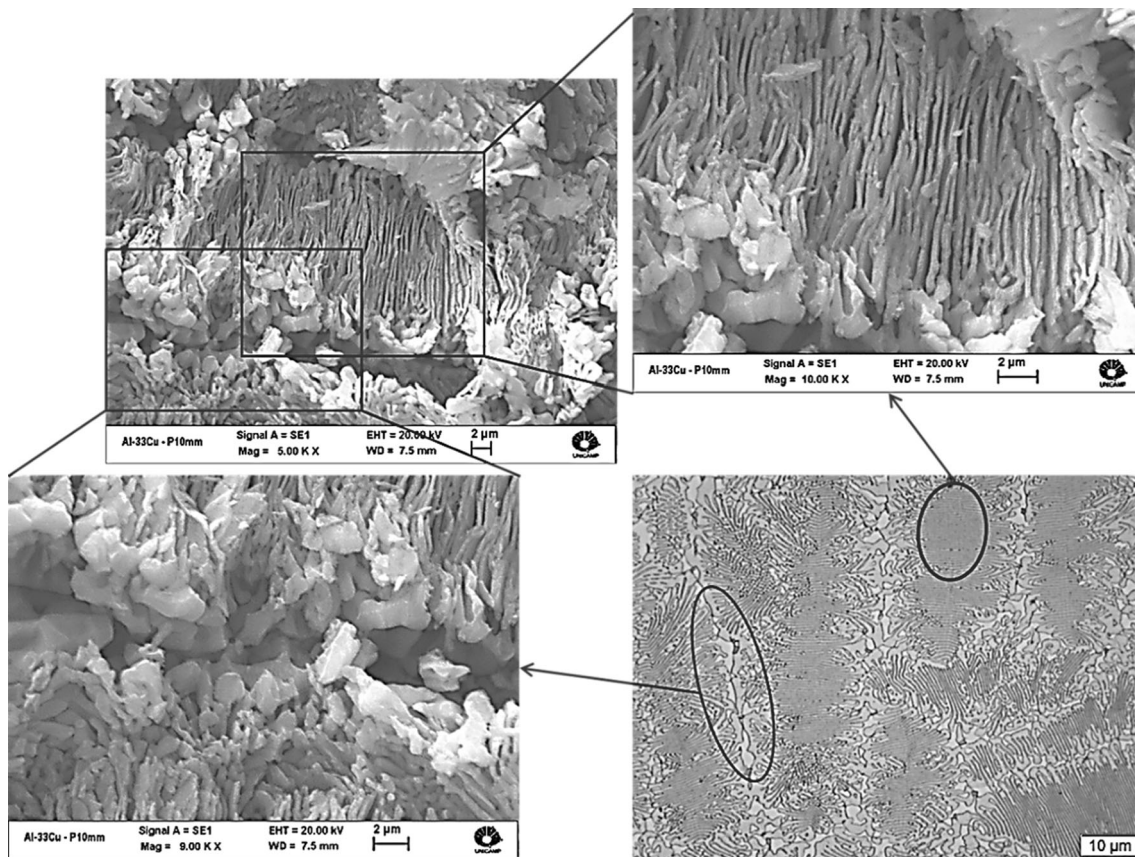


Fig. 4 right after the passage of the eutectic isotherm was calculated. So, the cooling rates could be determined as a function of position ( $P$ ) along the length of the Al–33 mass% Cu alloy casting. The two experimental variations in  $v_E$  and  $\dot{T}$  are shown in Fig. 10. The heating stage

observed in Fig. 4 due to gap formation in the metal/mold interface was converted in the experimental cooling rate points. It can be seen a certain stabilization of  $\dot{T}$  around  $5.0 \text{ K s}^{-1}$  for intermediate positions at 8 mm, 11.5 mm





**Fig. 8** SEM deep-etched microstructures of the Al-33 mass% Cu alloy for a cooling rate of  $4.9 \text{ K s}^{-1}$ . Details of the center and the boundary zones of the cells are outlined

and 17 mm from the cooled base of the casting, despite slight decrease in  $\dot{T}$ .

### Scaling laws, elemental distribution and hardness

The experimental variations in the eutectic colony spacing,  $\lambda_{EC}$ , the lamellar spacing,  $\lambda_L$ , and the coarser eutectic spacing,  $\lambda_E$ , as a function of  $v_E$  and  $\dot{T}$  are plotted in Fig. 11. For such, an overlap of data related to the evolution of  $v_E$  and  $\dot{T}$  and the measurements of spacings was performed. The evolution of the solidification kinetics clearly affects those spacings. Higher  $v_E$  and  $\dot{T}$  are associated with smaller  $\lambda$ .

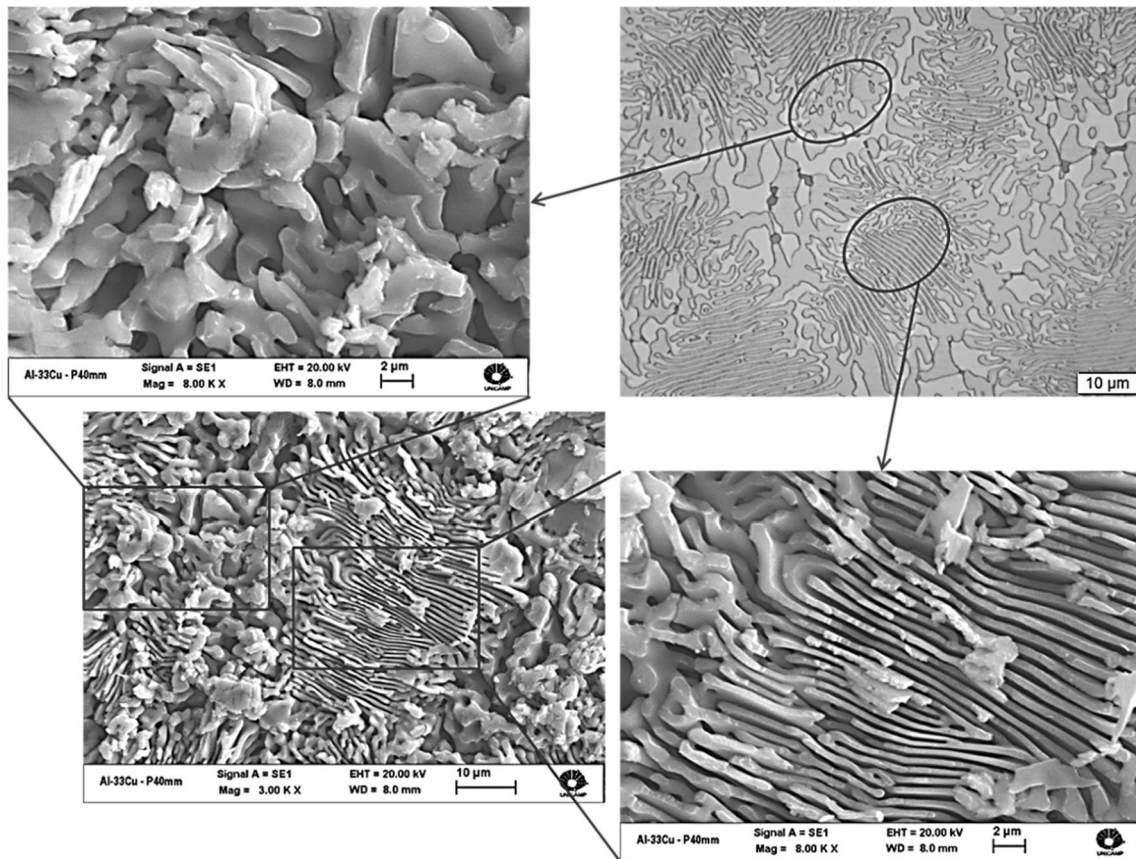
Even considering that a morphological transition happened during the growth of colonies in the Al-Cu eutectic alloy, a single exponent of  $-0.55$  showed to be representative of the entire range of colony spacings collected and related to the cooling rate, as shown in Fig. 11a. This exponent refers to the adjustment of a power function to the experimental scatter.

A previous research on hypoeutectic Al-Cu alloys with 5, 8 and 15 mass% Cu demonstrated that the experimental

law relating the primary dendritic spacing to the cooling rate was independent of composition if considered such range of Cu concentrations [43]. For comparison purposes, the derived growth law of such study is included in Fig. 11a. The analysis of the multipliers when comparing both compositions (i.e., 33 and 15 mass% Cu) allows affirming that much lower spacings characterize the eutectic Al-33 mass% Cu. This is so since the exponent in both experimental equations is preserved. This kind of comparison is very interesting in terms of the scale of the main spacings, despite the difference in the microstructural morphologies (primary dendritic spacings for hypoeutectic alloys and colony spacings for the eutectic alloy).

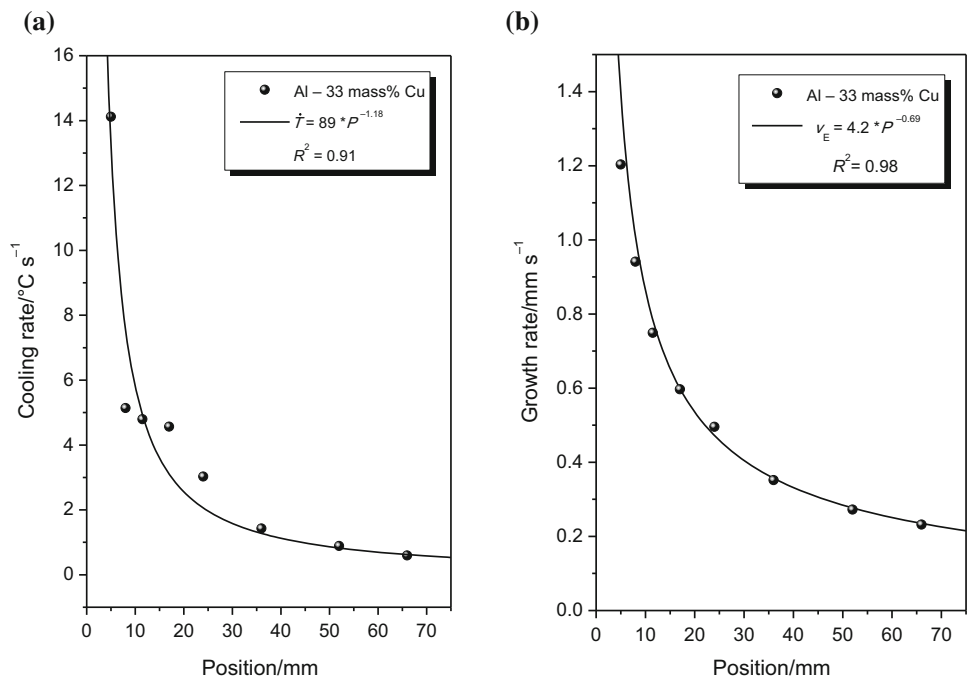
Both eutectic zones within the Al-Cu colonies have their growth laws  $\lambda$  versus  $v_E$  characterized by the  $-1/2$  exponent as shown in Fig. 11d, f. This is the same power function exponent as that originally proposed by Jackson and Hunt for the growth of regular eutectics [10]. The adopted exponent in the present results roughly agrees with those proposed by Stoichev et al. [14] for Fe contaminated Al-Cu eutectic alloys. These authors recommended that the exponent range governing the eutectic microstructure





**Fig. 9** SEM deep-etched microstructures of the Al–33 mass% Cu alloy for a cooling rate of  $1.1 \text{ K s}^{-1}$ . Details of the center and the boundary zones of the cells are outlined

**Fig. 10** Experimental profiles of **a** cooling rate and **b** eutectic growth rate for the directionally solidified Al–33 mass% Cu eutectic alloy.  $R^2$  is the coefficient of determination of the fitted curves



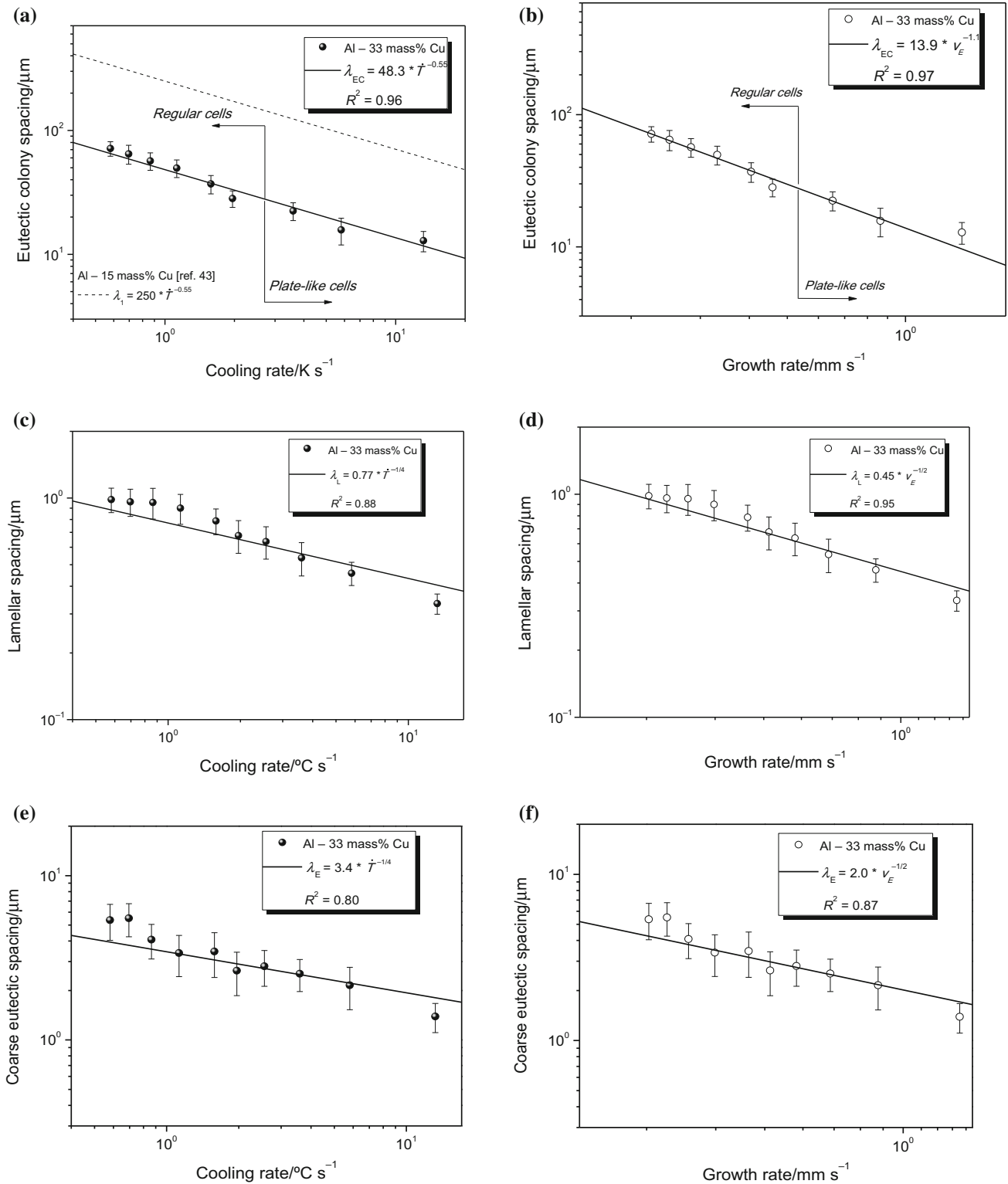


**Fig. 11** Experimental relationships of **a, b** eutectic colony spacing; **c, d** lamellar spacing; and **e, f** coarse eutectic spacing versus cooling rate and eutectic growth rate for the Al-33 mass% Cu alloy.  $R^2$  is the coefficient of determination

dispersion is characterized close to  $-1/2$ , varying from  $-0.41$  to  $-0.50$ .

A direct comparison between the eutectic length scales of lamellas and of coarse boundary structures of the eutectic Al-33 mass% Cu permitted to verify that the



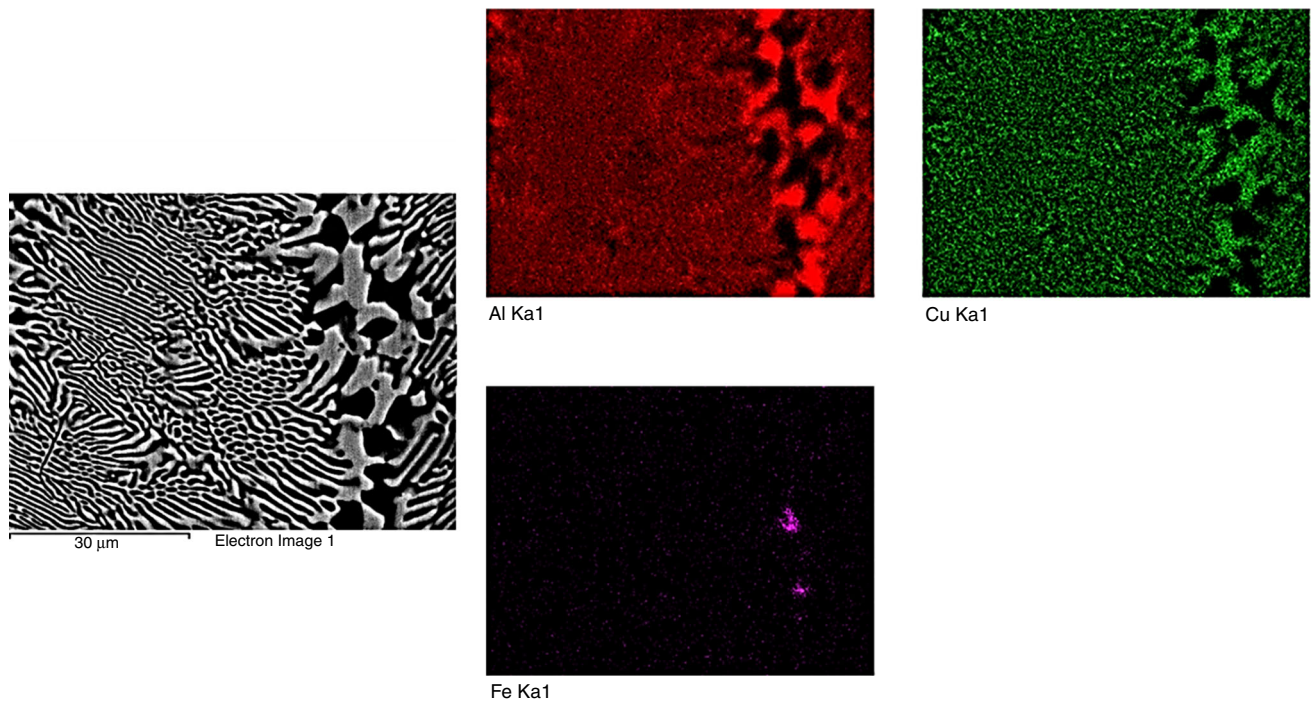


**Fig. 12** Elemental distribution by SEM–EDS area analysis in a sample of the directionally solidified Al–33 mass% Cu alloy casting

coarse eutectic spacing,  $\lambda_E$ , is of about 4.5 times larger than the lamellar spacing,  $\lambda_L$ .

In order to confirm the presence of iron in the microstructure as well as to operate as a guide for a point SEM–EDS examination, a previous elemental SEM–EDS mapping for the Al–33 mass% Cu alloy was performed. The final distribution of the elements is shown in Fig. 12, being clearer if considered the cellular boundary of the microstructure. The red contrast for Al shows a high intensity within the  $\alpha$ -Al eutectic phase, as expected, while the green for Cu is mainly concentrated in the  $Al_2Cu$  particles. Two spots highly concentrated in Fe can be noted in a third EDS mapping in Fig. 12. These regions have grown in the vicinities of the  $Al_2Cu$  particles constituting the coarse eutectic. Such spots will be next associated with the points #4 and #6 of the point EDS analyses in Fig. 13.

The SEM–EDS measurements shown in Fig. 13 confirm the growth of the Al– $Al_2Cu$  eutectic with basis on the composition of points #2 and #7. The compositions found for the EDS points #1, #3 and #5 emphasize the predominance of Al in the  $\alpha$ -Al eutectic phase composing the eutectic. Some of the points (#4 and #6) characterize the ternary AlFeCu intermetallic particles. Considering the atomic percentage of these points it is possible to deduce that this Fe-bearing intermetallic is the  $Al_7FeCu_2$ . Such measurements are related to the darker gray particles decorating the boundaries of the cells, as shown in Figs. 6 and 7.

The experimental solute distribution profiles of Fe and Cu within the Al–33 mass% Cu casting showed quite stable compositions for a number of specimens across the length of the directionally solidified body.

Figure 14 shows that the Cu concentration is essentially constant. This is due to the fact that Cu participates in the eutectic reaction, which is basically dominated by the lateral diffusion-coupled growth between phases [7, 10]. It appears that frontal segregation of Cu is very inhibited. On the other hand, despite the precipitation of the  $Al_7FeCu_2$  intermetallics, it seems that the local iron concentration ahead the solidification interface remains equalized and constant for the experienced growth conditions. As a result, Fe concentration is essentially constant.

The Vickers microhardness variation against the eutectic colony spacing is shown in Fig. 15 for the Al–Cu eutectic alloy. A tendency of increasing hardness is noted with decreasing  $\lambda_{EC}$ . Such tendency is mainly associated with the zone of predominance of platelike cells in the microstructure. In this region, a Hall–Petch-type correlation adjusts thoroughly. A decrease in the eutectic colony spacing means also a decrease in lamellar spacing and coarse eutectic spacing, which are other features characterizing the microstructure. As a consequence, the  $Al_2Cu$  reinforcing phase may be more homogeneously distributed throughout the microstructure. As such, hardness increases.

However, for low  $\lambda_{EC}^{-1/2}$ , where regular eutectic cells prevail, Vickers hardness remained essentially constant. This is explained by the comparative small variation in

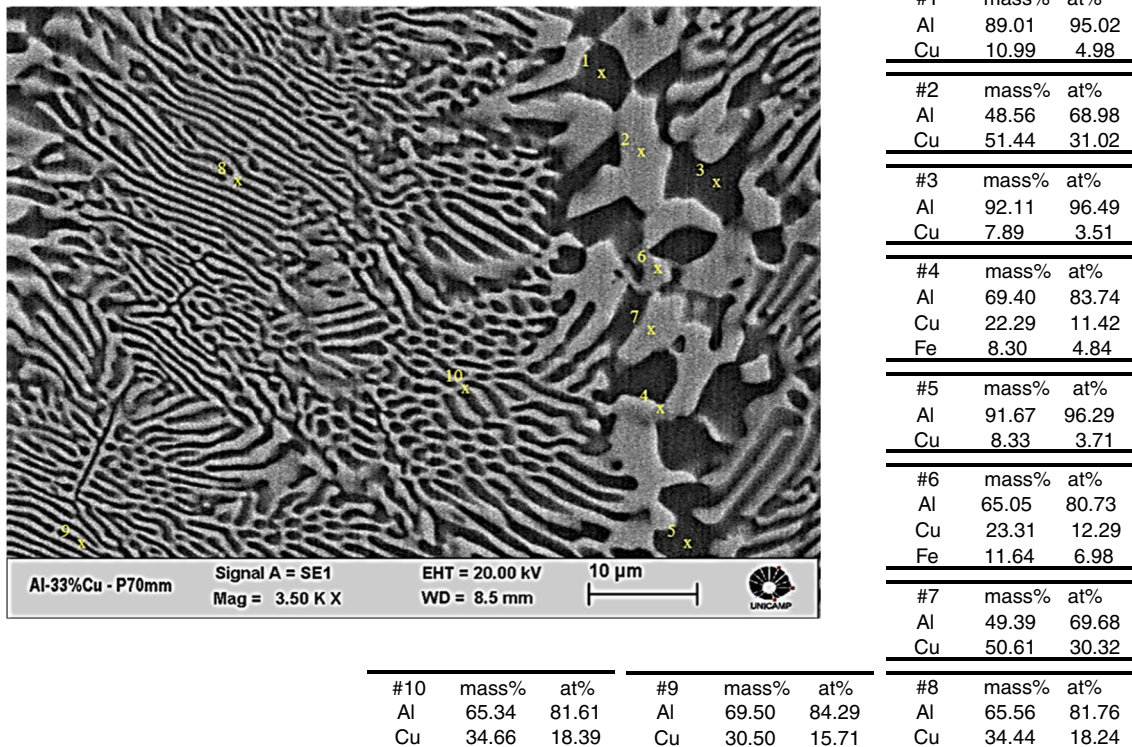


Fig. 13 SEM microstructure and point EDS measurements related to the position 70 mm from the cooled bottom of the Al–33 mass% Cu alloy casting

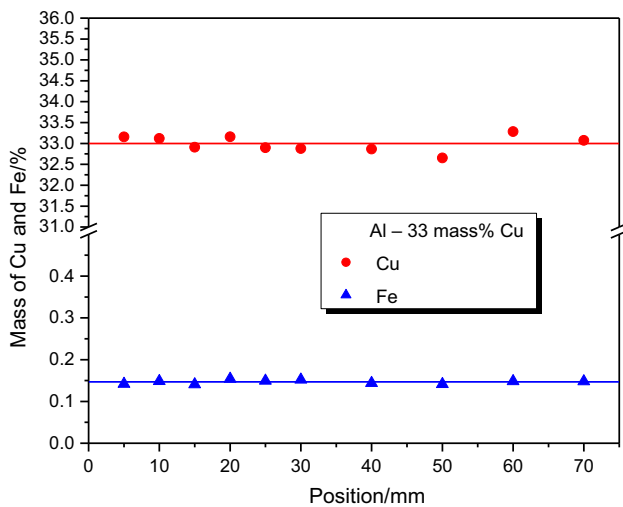


Fig. 14 Distributions of Cu and Fe along the length of the directionally solidified Al–33 mass% Cu alloy casting

length scale of the eutectic features such as the average eutectic colony spacing (from 39.0 to 71.0  $\mu\text{m}$ ) and the average lamellar spacing (from 0.70 to 0.98  $\mu\text{m}$ ). Such ranges of variation appear to be not enough to affect hardness of the Al–Cu eutectic alloy.

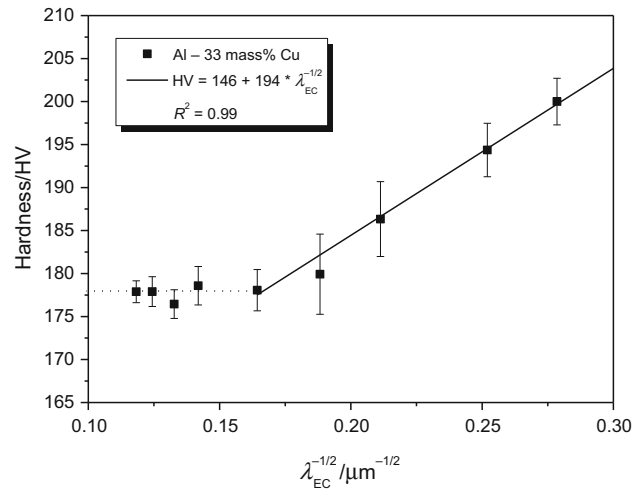


Fig. 15 Vickers hardness (HV) variation as a function of the eutectic colony spacing ( $\lambda_{EC}^{-1/2}$ ) for the Al–33 mass% Cu alloy casting.  $R^2$  is the coefficient of determination

### Conclusions

The following conclusions can be drawn from the present experimental investigation:

- The directionally solidified Al–33Cu alloy casting was shown to have very fine columnar grains prevailing



along the entire length of the casting. The microstructure is typified by eutectic cells having a predominance of lamellar  $\alpha$ -Al + Al<sub>2</sub>Cu eutectic. A bimodal distribution of Al–Al<sub>2</sub>Cu was shown to occur with very thin lamellas in the center of the cells, wavy lamellas and coarser random eutectic at the boundaries, which has been attributed mainly to the segregation of Fe. A platelike cellular morphology prevailed for  $v_E > 0.6 \text{ mm s}^{-1}$ .

- Experimental growth laws describing the evolutions of the eutectic colony spacing,  $\lambda_{EC}$ , the lamellar spacing,  $\lambda_L$ , and the coarser eutectic spacing,  $\lambda_E$ , as a function of  $v_E$  and  $\dot{T}$  have been proposed:

$$\lambda_{EC} = 48.3\dot{T}^{-0.55} \text{ and } \lambda_{EC} = 13.9 v_E^{-1.1}$$

$$\lambda_L = 0.77\dot{T}^{-1/4} \text{ and } \lambda_L = 0.45 v_E^{-1/2}$$

$$\lambda_E = 3.4\dot{T}^{-1/4} \text{ and } \lambda_E = 2.0 v_E^{-1/2}$$

where  $\lambda_{EC/L/E}$  is expressed in  $\mu\text{m}$ ,  $\dot{T}$  in  $\text{K s}^{-1}$  and  $v_E$  in  $\text{mm s}^{-1}$ .

- A Hall–Petch-type correlation has been proposed relating the evolution of Vickers hardness (HV) against the eutectic colony spacing,  $\lambda_{EC}$  along the region in the DS casting where platelike cells prevailed:

$$\text{HV} = 146 + 194 \lambda_{EC}^{-1/2}$$

The highest hardness of 200 HV is related to an ultrafine bimodal structure ( $\lambda_{EC} = 13 \mu\text{m}$ ). For low  $\lambda_{EC}^{-1/2}$ , where regular eutectic cells prevailed, and HV remained essentially constant (HV  $\sim$  178).

**Acknowledgements** The authors are grateful to FAPESP (São Paulo Research Foundation, Brazil: Grant 2017/12741-6) and CNPq - National Council for Scientific and Technological Development for their financial support.

## References

1. Stefanescu DM, Abbaschian GJ, Bayuzick RJ. Solidification processing of eutectic alloys. Warrendale: Metallurgical Society; 1988. ISBN 0873390334.
2. Campbell J. Castings. 2nd ed. Butterworth-Heinemann; 2003.
3. Silva BL, Garcia A, Spinelli JE. Complex eutectic growth and Bi precipitation in ternary Sn–Bi–Cu and Sn–Bi–Ag alloys. *J Alloys Compd.* 2017;691:600–5.
4. Elliot R. Eutectic solidification. *Int Met Rev.* 1997;22:161–86.
5. Tiller WA. Liquid metals and solidification. Cleveland: ASM; 1958.
6. Reyes RV, Bello TS, Kakitani R, Costa TA, Garcia A, Cheung N, Spinelli JE. Tensile properties and related microstructures aspects of hypereutectic Al–Si alloys directionally solidified under different melt superheats and transient heat flow conditions. *Mater Sci Eng A.* 2017;685:235–43.
7. Kaya H, Çadırılı E, Gündüz M, Ülgen A. Effect of the temperature gradient, growth rate, and the interflake spacing on the microhardness in the directionally solidified Al–Si eutectic alloy. *J Mater Eng Perform.* 2003;12:544–51.
8. Hosch T, England LG, Napolitano RE. Analysis of the high growth-rate transition in Al–Si eutectic solidification. *J Mater Sci.* 2009;44:4892–9.
9. Kakitani R, Reyes RV, Spinelli JE, Cheung N, Garcia A. Relationship between spacing of eutectic colonies and tensile properties of transient directionally solidified Al–Ni eutectic alloy. *J Alloys Compd.* 2018;733:59–68.
10. Jackson KA, Hunt JD. Lamellar and rod eutectic growth. *Trans Metall Soc AIME.* 1966;236:1129–42.
11. Çadırılı E, Ülgen A, Gündüz M. Directional solidification of the aluminium–copper eutectic alloy. *Mater Trans JIM.* 1999;40:989–96.
12. Ourdjini A, Liu J, Elliott R. Eutectic spacing selection in Al–Cu system. *Mater Sci Technol.* 1994;10:312–8.
13. Zimmermann M, Carrard M, Kurz W. Rapid solidification of Al–Cu eutectic alloy by laser remelting. *Acta Metall.* 1989;37:3305–13.
14. Stoichev NV, Yaneva SB, Regel LL, Videnskiy IV. Eutectic solidification of Al–Cu alloys influenced by convection. *Adv Space Res.* 1988;8:171–4.
15. Seetharaman V, Trivedi R. Eutectic growth: selection of inter-lamellar spacings. *MTA.* 1988;19:2955–64.
16. Zimmermann M, Carrard M, Gremaud M, Kurz W. Characterization of the banded structure in rapidly solidified Al–Cu alloys. *Mater Sci Eng A.* 1991;134:1278–82.
17. Yaneva S, Budurov S, Stoichev N, Chnistova S, Jonchev S. Eutectic crystallization of aluminium copper alloys (II). Influence of impurity elements. *Kris Tech.* 1975;10:395–400.
18. Zimmermann M, Karma A, Carrard M. Oscillatory lamellar microstructure in off-eutectic Al–Cu alloys. *Phys Rev B.* 1990;42:833–7.
19. Sahoo S, Ghosh S. Heat transfer, solidification, and microstructural evolution in Al–33Cu alloy during the starting of twin roll strip casting. *Steel Res Int.* 2014;85:207–18.
20. Tiwary CS, Mahapatra DR, Chattopadhyay K. Effect of length scale on mechanical properties of Al–Cu eutectic alloy. *Appl Phys Lett.* 2012;101:171901.
21. He G, Eckert J, Loser W, Schultz L. Novel Ti-base nanostructure-dendrite composite with enhanced plasticity. *Nat Mater.* 2003;2:33–7.
22. Park JM, Kim KB, Kim DH, Mattern N, Li R, Liu G, Eckert J. Multi-phase Al-based ultrafine composite with multi-scale microstructure. *Intermetallics.* 2010;18:1829–33.
23. Singh RK, Chattopadhyay K, Lele S, Anantharaman TR. Impact of substrate temperature on rapid solidification of an Al–Cu eutectic alloy. *J Mater Sci.* 1982;17:1617–22.
24. Bertorello HR, Biloni H. Structure and heat treatment influence on the tensile properties of Al–Al<sub>2</sub>Cu eutectic composites. *Metall Trans A.* 1972;3:73–82.
25. Meyers MA, Mishra A, Benson DJ. Mechanical properties of nanocrystalline materials. *Prog Mater Sci.* 2006;51:427–556.
26. Kashyap S, Tiwary CS, Chattopadhyay K. Effect of gallium on microstructure and mechanical properties of Nb–Si eutectic alloy. *Intermetallics.* 2011;19:1943–52.
27. Gunduz M, Çadırılı E. Directional solidification of aluminium–copper alloys. *Mater Sci Eng A.* 2002;327:167–85.
28. Çadırılı E, Büyük U, Engin S, Kaya H. Effect of silicon content on microstructure, mechanical and electrical properties of the directionally solidified Al-based quaternary alloys. *J Alloys Compd.* 2017;694:471–9.
29. Mondolfo LF. Aluminum alloys: structure and properties. London: Butterworth; 1976.

30. Mertinger V, Szabo G, Barczy P, Kovacs A, Czel G. Gravity influenced convection in Al–Ni melt. *Mater Sci Forum*. 1996;215(216):331–6.
31. Juarez-Hernandez A, Jones H. Growth temperature measurements and solidification microstructure selection of primary Al<sub>3</sub>Ni and eutectic in the  $\alpha$ Al–Al<sub>3</sub>Ni system. *Scr Mater*. 1998;38:729–34.
32. Moura ITL, Silva CLM, Cheung N, Goulart PR, Garcia A, Spinelli JE. Cellular to dendritic transition during transient solidification of a eutectic Sn 07 wt% Cu solder alloy. *Mater Chem Phys*. 2012;132:203–9.
33. Zhao S, Li J, Liu L, Zhou Y. Eutectic growth from cellular to dendritic form in the undercooled Ag–Cu eutectic alloy melt. *J Cryst Growth*. 2009;311:1387–91.
34. Walder S, Rayder PL. Critical solidification behavior of undercooled Ag–Cu alloys. *J Appl Phys*. 1993;74:6100–6.
35. Drevet B, Camel D, Dupuy M, Favier JJ. Microstructure of the Sn–Cu<sub>6</sub>Sn<sub>5</sub> fibrous eutectic and its modification by segregation. *Acta Mater*. 1996;44:4071–84.
36. Ventura T, Terzi S, Rappaz M, Dahle AK. Effects of solidification kinetics on microstructure formation in binary Sn–Cu solder alloys. *Acta Mater*. 2011;59:1651–8.
37. Han SH. Stability of a eutectic interface during directional solidification. PhD thesis, Iowa State University; 1995.
38. Tewari N, Raj SV, Locci IE. A Comparison between growth morphology of eutectic cells/dendrites and single-phase cells/dendrites. *Metall Mater Trans A*. 2004;35:1632–5.
39. Kurz W, Fisher DJ. Fundamentals of solidification. 3rd ed. Zurich: Trans Tech Publications; 1989.
40. Xu W, Feng YP, Li Y, Li ZY. Cellular growth of Zn-rich Zn–Ag alloys processed by rapid solidification. *Mater Sci Eng A*. 2004;373:139–45.
41. Ma D, Li Y, Ng SC, Jones H. Unidirectional solidification of Zn-rich Zn–Cu peritectic alloys—II. Microstructural length scales. *Acta Mater*. 2000;48:1741–51.
42. Vida A, Freitas ES, Brito C, Cheung N, Arenas MA, Conde A, Damborenea J, Garcia A. Thermal parameters and microstructural development in directionally solidified Zn-rich Zn–Mg alloys. *Metall Mater Trans A*. 2016;47:3052–64.
43. Rocha OFL, Siqueira CA, Garcia CA. Heat flow parameters affecting dendrite spacings during unsteady-state solidification of Sn–Pb and Al–Cu alloys. *Metall Mater Trans A*. 2003;34:995–1006.

**Publisher's Note** Springer Nature remains neutral with regard to jurisdictional claims in published maps and institutional affiliations.